HHS Public Access

Author manuscript

Mol Psychiatry. Author manuscript; available in PMC 2019 October 26.

Published in final edited form as:

Mol Psychiatry. 2019 November ; 24(11): 1732–1747. doi:10.1038/s41380-018-0048-y.

Critical Period Inhibition of NKCC1 Rectifies Synapse Plasticity in the Somatosensory cortex and Restores Adult Tactile Response Maps in Fragile X Mice

Qionger He[1], **Erica D Arroyo**[2], **Samuel N Smukowski**[3], **Jian Xu**[1], **Claire Piochon**[1], **Jeffrey N Savas**[3], **Carlos Portera-Cailliau**[2], **Anis Contractor**[1,4,*]

[1]Department of Physiology, Northwestern University Feinberg School of Medicine

[2]Departments of Neurology and Neurobiology, David Geffen School of Medicine at UCLA, Los Angeles, CA 90095

[3]Department of Neurology, Northwestern University Feinberg School of Medicine

[4]Department of Neurobiology, Weinberg College of Arts and Sciences, Northwestern University, Chicago, IL 60611

Summary

Sensory perturbations in visual, auditory and tactile perception are core problems in Fragile X Syndrome (FXS). In the *Fmr1* knockout mouse model of FXS, the maturation of synapses and circuits during critical period (CP) development in the somatosensory cortex is delayed, but it is unclear how this contributes to altered tactile sensory processing in the mature CNS. Here we demonstrate that inhibiting the juvenile chloride co-transporter NKCC1, which contributes to altered chloride homeostasis in developing cortical neurons of FXS mice, rectifies the chloride imbalance in layer IV somatosensory cortex neurons and corrects the development of thalamocortical excitatory synapses during the CP. Comparison of protein abundances demonstrated that NKCC1 inhibition during early development caused a broad remodeling of the proteome in the barrel cortex. In addition, the abnormally large size of whisker-evoked cortical maps in adult *Fmr1* knockout mice was corrected by rectifying the chloride imbalance during the early CP. These data demonstrate that correcting the disrupted driving force through $GABA_A$ receptors during the CP in cortical neurons restores their synaptic development, has an unexpectedly large effect on differentially expressed proteins, and produces a long-lasting correction of somatosensory circuit function in FXS mice.

Correspondence: Anis Contractor, Department of Physiology, Northwestern University Feinberg School of Medicine, 303 E. Chicago Ave, Chicago, Il 60611, a-contractor@northwestern.edu, Tel: 312 503 1843 Fax: 312 503 5101.

*Lead Contact

Author Contributions: QH, EA, SNS, CP performed experiments, analyzed data, and contributed to writing of the manuscript. JNS, CP-C and AC provided direction for the study, analyzed data, and wrote the manuscript. CP-C and AC generated funding to support the experiments. All authors contributed to the conception and design of the experiments.

The authors have no conflicts of interest to declare.

Keywords

Fragile X Syndrome; critical period; NKCC1; bumetanide; synapse

Introduction

Fragile X syndrome (FXS) is a prevalent neurodevelopmental disorder that is the leading genetic determinant of intellectual disability and autism. It results from *FMR1* gene silencing and the subsequent loss of the translational suppressor fragile X mental retardation protein (FMRP)[1]. FMRP regulates the translation of a large number of neuronal transcripts[2] and the loss of this regulation in FXS impairs synapse development and results in the formation of aberrant neuronal circuits that affect brain function[3]. Delays in early developmental milestones are reported in Fragile X patients[4] suggesting that early vulnerable periods are particularly important in the disorder.

Sensory hypersensitivity is a prominent symptom of FXS that can manifest behaviorally as tactile defensiveness and avoidance of normally non-aversive sensory stimuli[5, 6]. Sensory disturbances can lead to many associated behavioral deficits such as hyperarousal, anxiety, and social withdrawal. Hence, correction of sensory hypersensitivity has the potential to significantly improve the lives of patients. The *Fmr1* knockout (KO) mouse model of FXS also exhibits heightened sensory responses to both auditory[7] and tactile stimuli[8–10] as well as numerous alterations in the development of synapses and circuits in the somatosensory cortex[11–15]. In particular, it has been demonstrated that there is a delay in the development of synapses formed between the primary sensory input into the cortex from the thalamus to layer IV spiny stellate neurons of somatosensory cortex in *Fmr1* KO mice. In typically developing mice, these glutamatergic synapses mature during the first postnatal week through activity dependent incorporation of AMPA receptors (AMPAR), resulting in a reduction of NMDA receptor-only (NMDAR)-only silent synapses[16]. In *Fmr1* KO mice, abnormal retention of silent synapses persists beyond the first postnatal week and results in a shifted time window for NMDAR dependent critical period (CP) plasticity[12]. It is during this CP that the developing cortical network is most responsive to modification by sensory perturbation, and connections are refined for the correct construction of the mature sensory network[17]. However, whether the altered timing of the CP window early in postnatal development leads to disruptions in the emergent properties of the network and contributes to changes in sensory evoked responses in the mature cortex is not known.

In addition to the proper sequence of glutamatergic synapse development during the CP, there is a parallel delay in the maturation of the $GABA_A$ receptor equilibrium potential (E_{GABA})[18]. E_{GABA} sets the efficacy of GABA transmission and the immature depolarized reversal potential has been proposed to have trophic effects on the developing central nervous system (CNS)[19]. E_{GABA} becomes increasingly hyperpolarized in many neuronal types with age, which affects the driving force through $GABA_A$ receptors[20]. This developmental change is mediated by alterations in intracellular chloride $[Cl^-]_{INT}$ which is maintained by the expression of two Cl^- co-transporters; Na^+-K^+-Cl^- co-transporter (NKCC1) is expressed early in development and elevates $[Cl^-]_{INT}$, and K^+-Cl^- co-

transporter (KCC2) expresses at increasing levels later in development and which extrudes Cl^- from the cell[21]. *Fmr1* KO mice have an abnormally high expression of NKCC1 in the cortex at P10, which coincides with the end of the CP[18]. This high expression of NKCC1 could primarily drive the prolonged depolarized E_{GABA} in layer IV neurons. Because GABA-mediated depolarization can directly induce synaptogenesis and the maturation of glutamatergic synapses[22, 23], mistimed maturation of E_{GABA} may cause the aberrant development of glutamatergic synapses in *Fmr1* KO mice. But as yet, it has not been demonstrated whether the prolongation of a depolarized E_{GABA} during the CP is causally related to the altered development of excitatory synapses in the somatosensory cortex in *Fmr1* KO mice.

Here we demonstrate that daily administration of the NKCC1 inhibitor, bumetanide, to *Fmr1* KO mice corrected E_{GABA} in principal neurons of the barrel cortex. More importantly, this treatment regime simultaneously corrected the developmental trajectory of excitatory synapses and the CP time window for synaptic plasticity of thalamocortical synapses in layer IV neurons. We found a significant proteome-wide adaptation in bumetanide treated animals that demonstrated that the drug caused a large reorganization in the level of many proteins, including those with known synaptic function and developmental roles. Moreover, when mice were administered bumetanide only during CP development, the enlarged whisker response maps in barrel cortex were corrected and remained corrected in adult *Fmr1* KO mice. Therefore, correcting E_{GABA} during CP development is sufficient to normalize the properties of the mature sensory network in the CNS of *Fmr1* KO mice.

Results

Bumetanide treatment rectifies E_{GABA} in the cortex at the end of the critical period

In *Fmr1 KO* mice, the equilibrium potential for GABA is relatively depolarized during the CP and the expression of the juvenile chloride co-transporter NKCC1 is abnormally elevated at the close of the CP in layer IV at postnatal day 10 (PND 10)[18]. To determine whether systemic administration of the NKCC1 inhibitor bumetanide could act centrally to correct E_{GABA}, *Fmr1* KO mice (*Fmr1*$^{-/y}$) and littermate *Fmr1* WT controls (*Fmr1*$^{+/y}$) were treated with daily intraperitoneal (i.p.) injections of bumetanide (0.2 mg/kg)[24, 25] or vehicle (see Experimental Procedures) beginning at PND 0 until the day of experimentation (Figure 1A). At PND 10 thalamocortical slices were prepared[12] and gramicidin perforated patch recordings were made from visually identified layer IV spiny stellate neurons. Measurement of $GABA_A$ mediated currents at several holding membrane potentials (Vm) were made, and E_{GABA} extrapolated from the x-axis intersect of the constructed current-voltage (I-V) relationships. In vehicle-treated *Fmr1* WT mice at P10 E_{GABA} was −75.6 ± 3.2 mV, n = 10/4 (cells/mice) and this was not different from E_{GABA} measured in *Fmr1* WT mice treated with bumetanide for 10 days (−73.3 ± 2.2 mV, $F_{1,36} = 0.19$, p = 0.67, n=12/3, two-way ANOVA with Bonferroni adjustment; Figure 1B–D). In contrast, in recordings from vehicle treated *Fmr1* KO mice we found E_{GABA} to be significantly depolarized at PND 10 (−51.8 ± 4.8 mV, n = 14/5) in comparison to vehicle treated *Fmr1* WT (−75.6 ± 3.1 mV, $F_{1,44} = 21.1$, p = 0.00004 n = 10/4, two-way ANOVA with Bonferroni adjustment)(Figure 1C–D), which is in agreement with our previous findings of a relatively depolarized E_{GABA} in *Fmr1* KO mice[18].

Most importantly, the *Fmr1* KO group treated daily with bumetanide had an average E_{GABA} that was more hyperpolarized than in the vehicle-treated KO mice (−73.0 ± 3.4 mV, $F_{1,36}$ = 18.5 p = 0.0001, n = 12/4, two-way ANOVA with Bonferroni adjustment and which was not different to the WT level (p = 1.00 Kruskal-Wallis H test for pairwise comparison adjusted by the Bonferroni correction for multiple tests). The average resting membrane potential (RMP) was not significantly different between all the groups, and repeated postnatal bumetanide treatment normalized E_{GABA} to values more hyperpolarized than the average RMP in *Fmr1* mutant mice (RMP = −59.2 ± 2.1 mV, n = 4/3).

To ensure that repeated treatment over the course of the CP was necessary to produce the shift in E_{GABA} in the mutant mice, we performed two further experiments. We first administered bumetanide from P0-P9 and allowed at least 24 hours washout before slice preparation and recording (Figure 1A, orange regime). With this regimen, bumetanide was effective in hyperpolarizing E_{GABA} in layer IV neurons of PND 10 *Fmr1* KO mice to values comparable to bumetanide treated *Fmr1* WT mice at PND 10 (Figure 1E). In contrast, *Fmr1* KO mice treated with a single dose of bumetanide on the day of the experiment (PND 10, 2 hours prior to slice preparation) (Figure 1A, green regime) had a significantly depolarized E_{GABA} in neurons compared to 0–9 day treatment of bumetanide (P0–9 group, E_{GABA} = −70.8 ± 2.7 mV; single dose P10 group −45.3 ± 2.4 mV, n = 10/3 $F_{1,35}$ = 56.1, p = 1×10^{-8} n =9/3, two-way ANOVA with Bonferroni adjustment), and bumetanide treated *Fmr1* WT (–66.6 ± 2.0 mV in WT, n = 11/3, $F_{1,35}$ = 43.5 p = 1.3×10^{-7}, two-way ANOVA with Bonferroni adjustment, Figure 1E). This demonstrates that only repeated treatment with bumetanide through the CP corrects E_{GABA} in layer IV neurons of PND 10 *Fmr1* KO mice.

To further test whether the effect on E_{GABA} could be attributed directly to NKCC1 inhibition, we utilized a different NKCC1 inhibitor, the loop diuretic furosemide (20 mg/kg daily for 10 days), as well as mannitol (750 mg/kg daily for 10 days), which has no known activity on the chloride co-transporters[26] (Figure 1F). Furosemide treatment of *Fmr1* KO mice mimicked the effect of bumetanide and the measured E_{GABA} at P10 was relatively hyperpolarized (E_{GABA} = −68.9 ± 3.4 mV, n= 10/3; Figure 1F, G). In contrast, recordings from mannitol treated *Fmr1* KO mice demonstrated that E_{GABA} was depolarized in layer IV neurons at P10 (−34.0 ± 3.9 mV, n =8/3 p = 0.00001 unpaired *t*-test; compared to the furosemide group; Figure 1F, G). Together these data demonstrate that treatment of mice with an inhibitor of NKCC1 is effective at correcting the abnormal GABA equilibrium potential at the closure of the CP in *Fmr1* KO mouse cortex.

The development of excitatory synapses during the critical period is corrected by NKCC1 inhibition

The development of excitatory synapses in layer IV neurons is altered in *Fmr1* KO mice; the NMDAR:AMPAR (N:A) current ratio in thalamocortical synapses is abnormally high at the end of the first postnatal week, which is due to the retention of NMDAR-only immature silent synapses[12]. To record thalamocortical excitatory inputs to layer IV neurons, we stimulated the ventrobasal thalamus and isolated the evoked EPSCs in slices. At PND 7, the N:A ratio in vehicle-treated *Fmr1* KO mice was elevated (1.05 ± 0.12, n = 10/7) in comparison to the vehicle treated *Fmr1* WT group (0.60 ± 0.06, n = 10/4, $F_{1,36}$ = 8.9 p =

0.005 two-way ANOVA with Bonferroni adjustment; Figure 2 A, B), consistent with our previous report[12]. In *Fmr1* KO mice treated with bumetanide for seven days, the measured N:A ratio was lower compared to the vehicle treated (*Fmr1* KO group: 0.62 ± 0.14, n = 10/8, $F_{1,36}$ = 7.7 p = 0.009, two-way ANOVA with Bonferroni adjustment), which was similar to the N:A ratio in vehicle treated *Fmr1* WT mice (0.60 ± 0.06, n = 10/4, p = 0.693, two-way ANOVA with Bonferroni adjustment; Figure 2A, B). In recordings from mice at each postnatal day between PND 5 and PND 11, we found that the normal developmental decline in N:A ratio over this period was restored in *Fmr1* KO mice treated with bumetanide daily from PND 0 (Figure 2D). Bumetanide treatment in *Fmr1* WT mice had no effect on the N:A ratio (Figure 2C).

Persistence of silent synapses and LTP are corrected by bumetanide administration

The elevated N:A ratio of thalamocortical synapses is reflective of a retention of NMDAR-only silent synapses at the closure of the CP for layer IV at PND 7 in *Fmr1* KO mice[12]. We next tested whether bumetanide treatment had any effects on the relative number of NMDAR-only synapses. Minimal stimulation of thalamocortical connections was used to assess the failure rate in layer IV neurons while voltage clamping neurons at −70mV or +40mV, and the failure ratio was calculated (failures at −70mV/failures at +40mV) as an indicator of the relative number of silent synapses, as previously described[12, 27]. At PND 7, vehicle treated *Fmr1* KO mice had a higher failure ratio (1.47 ± 0.19 n = 15/3) in comparison to recordings from vehicle treated *Fmr1* WT (0.70 ± 0.09, n = 12/3, p = 0.006 Kruskal Wallis test adjusted by the Bonferroni correction for multiple tests) reflecting a relatively larger proportion of NMDAR-only silent synapses (Figure 3A, C) consistent with our previous report[12]. The failure ratio measured in *Fmr1* WT mice was not different from that in the vehicle *Fmr1* WT group. However, the failure ratio in the drug treated *Fmr1* KO group was significantly lower compared to vehicle treated *Fmr1* KOs (0.83 ± 0.14, n = 14/3, p = 0.023 compared to the vehicle group 1.47 ± 0.19, n = 15/3 Kruskal-Wallis H test for pairwise comparison adjusted by the Bonferroni correction for multiple tests; Figure 3A–C). The lower failure ratio suggests that the relative number of silent synapses is reduced by bumetanide treatment, which is consistent with the reduction in N:A ratio in bumetanide treated animals. These findings indicate that NKCC1 inhibition corrects aberrant developmental maturation of excitatory synapses in layer IV neurons in *Fmr1* KO without impacting the maturation of synapses in *Fmr1* WT mice.

In addition to the retention of a greater number of NMDAR-only synapses at the closure of the CP, layer IV excitatory synapses remain plastic in *Fmr1* KO mice at a postnatal time when long term potentiation (LTP) does not occur in WT mice[16]. As this developmental plasticity is dependent on NMDARs and correlates with the fraction of silent synapses [27], we tested whether this synaptic phenotype was also corrected in *Fmr1* KO mice by bumetanide. Perforated patch voltage-clamp recordings were made at PND 7 and LTP was induced by a pairing of repetitive presynaptic thalamic activity and postsynaptic depolarization[12]. In both vehicle- and bumetanide-treated *Fmr1* WT mice, no LTP was observed at this age (Figure 3D). In contrast, there was a significant potentiation of the EPSC 30–40 minutes after LTP induction in vehicle treated *Fmr1* KO mice (131 ± 7.0%, n = 13/7, p = 0.001, unpaired *t*-test). There was no such potentiation in the bumetanide-treated

Fmr1 KO group but rather a modest LTD (88.5 ± 4.9, n = 8/7 p = 0.036 unpaired *t*-test), consistent with a normalization of synapses (Figure 3E). To fully determine the effect of bumetanide on LTP over the course of the CP we made further recordings at each PND 5–11. As we previously demonstrated for *Fmr1* mutant mice[12], we again found that, in vehicle-treated *Fmr1* KO mice, the normal time-course of LTP was disrupted over this period peaking abnormally at a later PND (Figure 3F). However, bumetanide treatment in *Fmr1* KO mice corrected this profile so that LTP was robust at the youngest ages (PND5: 121.8 ± 6.4 %, n= 14/6, compared to 98.7 ± 6.8 % n = 12/7 in vehicle *Fmr1* KO p =0.02 unpaired *t*-test) but potentiation disappeared by PND 7 and modest depression was again observed (88.5 ± 4.9%, n = 8/7; p = 0.037, unpaired *t*-test; Figure 3F). As we had observed in other experiments in *Fmr1* WT mice, there was no effect of bumetanide on LTP measured at any age when compared to vehicle group (Figure 3F, transparent lines). As a control for the specificity of bumetanide, we again utilized furosemide and mannitol. In *Fmr1* KO mice, the N:A ratio was 0.49 ± 0.08, n = 9/3 in bumetanide treated mice, while in the mannitol treated group the N:A ratio remained relatively high (0.98 ± 0.04, n = 8/3 p = 0.0001, unpaired *t*-test; Figure S1A–B). In addition, in *Fmr1* KO mice at PND 7, thalamocortical LTP was absent in the furosemide treated group (80.6 ± 5.0 %, n = 8/3) but persisted in the mannitol group (129.5 ± 10.9 %, n = 9/4; Figure S1C–D).

The proteome in the somatosensory cortex is altered by bumetanide treatment

FMRP is a RNA-binding protein that potentially regulates hundreds of RNAs directly and which, through actions on other translational regulators, has indirect effects on the expression and stability of an unknown number of others. Therefore, both direct and pleiotropic effects on the abundances of proteins are expected from loss of FMRP in FXS. Prior work has demonstrated a large number of differentially expressed proteins in *Fmr1* KO mice[28], therefore we wondered how bumetanide administration might affect the sensory cortical proteome in the barrel cortex of *Fmr1* KO. In order to compare protein expression of *Fmr1* KO and *Fmr1* WT mice, we performed ten-plex tandem mass tag (TMT) quantitative mass spectrometry (MS)[29] (see Methods). Mice were administered drug or vehicle from PND 0–14 covering the CP when E_{GABA} is relatively depolarized in *Fmr1* KO mice[18]. Mice were sacrificed at P17 and tissue samples collected from punches of the barrel cortex and processed for analysis[30]. Differentially expressed proteins were quantified by comparing the normalized average reporter ion intensities of peptides among the biological replicates from *Fmr1* KO mice and *Fmr1* WT mice (Figure 4A). Proteome quantification was robust, and we were able to quantify 3,929 proteins in the vehicle treatment group and 3,305 proteins in the bumetanide treatment group (Supplementary Table 1). 210 of the 3,929 proteins were significantly differentially expressed between *Fmr1* KO and *Fmr1* WT in the vehicle groups (*p* values in the range 0.0499 to 1.40×10^{-7}, Student's *t*-test, Supplemental Table 1), and therefore were presumably dysregulated by the absence of FMRP. In the bumetanide groups 761 of the 3,305 proteins were significantly differentially expressed between *Fmr1* KO and *Fmr1* WT (*p* values in the range 0.0499 to 1.72×10^{-7}, Student's *t*-test, Supplemental Table 1) (Figure 4B and 4C). In order to determine how bumetanide was altering the proteome we analyzed all those proteins significantly altered in the bumetanide datasets and compared them to their relative levels in the vehicle groups (i.e. genotype vs drug effects) (Supplemental Table 2). This comparison showed that the majority of proteins that were

significantly altered in the bumetanide comparison were not significantly altered in the vehicle comparison (673 out of 761)(Figure 4D)(Supplemental Table 2). However, 21 proteins that were significantly overexpressed in the bumetanide groups had demonstrated significant underexpression in the vehicle groups. Amongst these were important proteins parvalbumin (*Pvalb*) and TrkB receptor (*Ntrk2*), both known to be important for interneuron development. In the group of proteins found to be downregulated in the bumetanide group, only 5 had been overexpressed in the vehicle group, one of which was the important cell adhesion molecule L1 (Figure 4D). When we analyzed all the proteins that were non-significant in the bumetanide group, again only a small fraction of these had been significantly different in the vehicle groups (122 out of 2544) (Figure 4D, lower panel). 71 proteins that were overexpressed in the vehicle treated groups were normally expressed in the bumetanide treated groups, including several proteins known to important for developmental disorders such as *MeCP2* and *Rab3gap2*. Additionally, 51 of the proteins that were non-significant in bumetanide groups were underexepressed in the *Fmr1* KO in the vehicle treated comparison (Figure 4D, lower panel). In comparing the relative numbers of significantly altered proteins in vehicle or bumetanide treated datasets, we found more proteins were upregulated in the bumetanide groups (Figure 4E, bottom panel). We also compared our list of differentially expressed proteins to those whose mRNAs have been demonstrated to be FMRP targets[2]. Again the largest group of proteins belonging to this list of identified FMRP targets were upregulated in bumetanide treated mice (Supplemental Table 3). In both the vehicle and bumetanide groups multiple proteins that were previously found to be robust FMRP targets were identified to be significantly altered; however, this group was just a fraction of the more than 800 putative mRNA targets[2] (Figure 4E, top and Supplemental Table 3). Organizing the significantly altered proteins for functional assignment using the Panther statistical overrepresentation test[31] we found that, in the bumetanide treated groups, the significantly differentially expressed proteins were involved in metabolism and the synaptic vesicle cycle in the most significantly enriched categories (Figure 4F).

Whisker evoked responses in the cortex are normalized by repeated bumetanide treatment during the critical period

Prior work has demonstrated that there is a heightened neural response in the adult barrel cortex of *Fmr1* KO mice to tactile whisker stimuli[8–10]. We used optical imaging of intrinsic signals (OIS) to measure the cortical response to single whisker stimulation in order to determine whether sensory responses were affected by recurring bumetanide treatment during the CP. *Fmr1* KO and littermate *Fmr1* WT mice were administered bumetanide (0.2mg/kg) or vehicle during the first two postnatal weeks when E_{GABA} is more depolarized in *Fmr1* KO mice than WT littermates[18] (daily from PND 0 to PND 14)(Figure 5A). At PND14, mice underwent surgeries to implant cranial windows over the somatosensory cortex and imaging was first performed at PND 16/17 and then again at 2 months of age (in the same animals). The sensory representation map evoked by high frequency (100Hz, 1.5s) stimulation of the D2 whisker was measured in all the groups. At PND16/17, the vehicle-treated *Fmr1* KO group had a significantly larger cortical response (thresholded area) compared to vehicle-treated *Fmr1* WT controls (2396 ± 336 μm^2 vs. 1124 ± 311 μm^2, respectively, p = 0.003, two-way ANOVA with Bonferroni adjustment; Figure 5 B–D),

demonstrating that the previously reported increase in map size in 3 month old *Fmr1* KO mice[8] is already apparent by 2 weeks of age. In the bumetanide-treated *Fmr1* KO group the cortical whisker response was significantly reduced and indistinguishable from that of either the vehicle- or drug-treated WT animals (892 ± 68 μm^2 $p = 0.992$ vs WT two-way ANOVA with Bonferroni adjustment; Figure 5 B–D). Therefore, the enhanced sensory response in juvenile *Fmr1* KO mice can be normalized by bumetanide treatment. To determine whether drug administration during the CP has long lasting effects on cortical responses, we also measured the whisker-evoked intrinsic signals in the same animals at 2 months of age. Vehicle-treated adult *Fmr1* KO mice also had abnormally large cortical representations of whisker responses in comparison to the vehicle-treated *Fmr1* WT mice ($p = 1 \times 10^{-6}$, two-way ANOVA with Bonferroni adjustment; Figure 5 E–G). However, in the group treated with bumetanide during the CP the OIS neural activity map was no different from the WT groups (map area WT bumetanide vs KO bumetanide, $p = 0.21$, two-way ANOVA with Bonferroni pairwise comparisons). Therefore, bumetanide treatment during the early cortical CP corrects the circuit response to sensory whisker stimulation, an effect that persists through adulthood despite cessation of drug administration.

Discussion

In this study, we demonstrate that systemic administration of the FDA-approved diuretic bumetanide, an NKCC1 inhibitor, during a vulnerable stage of brain maturation can rectify developmental synaptic phenotypes that are prominent during CPs in the somatosensory cortex, as well as circuit function in mature sensory cortex of *Fmr1* KO mice. We found that repeated once-daily administration of bumetanide was sufficient to recue chloride homeostasis such that E_{GABA}, which is abnormally depolarized in layer IV neurons of *Fmr1* KO cortex, was restored to WT levels. Considering that disruption of chloride homeostasis has been reported in animal models of several neurodevelopmental disorders including Down Syndrome[32] and Rett Syndrome[33, 34], our results could have broad implications for a number of developmental disorders.

Our previous work had confirmed that E_{GABA} is depolarized in cortical neurons and that there was a correlated elevation in the relative expression of the juvenile chloride transporter NKCC1. Here we found that inhibition of NKCC1 by bumetanide, which only weakly penetrates the blood brain barrier[35] and has a relatively short half life[36], was effective in causing a hyperpolarization of the E_{GABA} at PND10 in the *Fmr1* KO mice. A single dose of bumetanide at PND10 did not have the same effect demonstrating that repeated dosing to block NKCC1 during the CP is required to achieve E_{GABA} rescue. Importantly, bumetanide had no apparent effect on E_{GABA} in neurons of WT mice. This is consistent with previous electrophysiological studies in brain slices from the Down Syndrome mice in which bumetanide affected E_{GABA}[32] In contrast to this the suppression of NKCC1 activity during embryonic development before cortical precursor cells have migrated to the cortex has a dramatic and deleterious effect[19].

Our primary motivation for determining whether E_{GABA} could be corrected by bumetanide was to test whether there is a causal relationship between altered GABA signaling and the development of synapses during the CP. We showed that the coordinated maturation of

glutamatergic inputs onto layer IV neurons is altered during the CP[12]. During the course of the first postnatal week, these synapses have a systematic decrease in their NMDAR content as synapses mature and NMDAR-only silent synapses are replaced by AMPAR containing synapses [27]. This process is delayed in *Fmr1* KO mice and the developmental LTP of thalamocortical synapses is prolonged beyond the end of the CP[12]. Correction of the $GABA_AR$ driving force with repeated bumetanide treatment completely normalized the developmental time-course of the N:A ratio and LTP and the persistence of silent synapses. This supports a causal relationship for the depolarized GABA reversal potential in synapse maturation during the CP in the somatosensory cortex. Interestingly a previous study demonstrated that bumetanide treatment of rats can prolong the CP in the visual cortex through an effect on BDNF and GABAergic synapses[24]. This indicates that altering E_{GABA} can have multiple effects on the normal maturation and development of different sensory areas. Depolarizing GABA and the associated effects on GABA efficacy can have both circuit and cellular effects [19]. For instance, there is evidence that depolarizing GABA in developing neurons contributes to unsilencing of glutamatergic synapses by being the primary source of membrane depolarization for the relief of the voltage dependent Mg^{2+} block of NMDARs [22]. This simple idea seems unlikely to be the case here as we would expect prolongation of depolarizing GABA to have the contrary effect to what we observed, i.e. reduce the number of silent synapses. Alternatively, shifts in E_{GABA} can affect the excitability of neurons in developing circuits causing changes in calcium dependent signaling pathways, gene expression and protein turnover[37]. Therefore, it remains to be determined how the dysregulated timing of E_{GABA} maturation, and the extent of the shift in GABA driving force, directly correlate with the extent of synaptic alterations in *Fmr1* KO mice.

We also used MS to determine the effects of bumetanide on the proteome. Previous work has demonstrated that the synaptic proteomes of *Fmr1* KO and WT mice diverge significantly during early development [28]. Different proteins are either upregulated and downregulated in the brain of mutant mice, reflecting both direct effects of FMRP loss and pleiotropic effects of the gene[28]. We, too, found a divergence of the proteome in tissue isolated from the barrel cortex of FXS mice. Even more dramatic effects were observed in protein expression in the bumetanide treated groups with more significantly altered proteins found in these groups. However, only a small number of proteins were “corrected” (i.e. those under- or over-expressed in vehicle that are normally expressed in the bumetanide groups). However, amongst these were some interesting proteins known to be involved in neurodevelopmental disorders (e.g. MeCP2[38]) or neuronal development and plasticity (e.g. GAP43[39]). We also found that a number of interesting proteins that were overexpressed in the bumetanide group, were underexpressed in the vehicle comparison. In particular, both parvalbumin (PV) and TrkB were in this category, and are noteworthy because of their roles in interneuron development[40]. Interestingly, it has recently been demonstrated that the development of PV expressing interneurons is disrupted in both the somatosensory and auditory cortices in *Fmr1* KO mice[41, 42] and can be rescued by activation of TrkB[42]. Broad changes in protein expression might reflect circuit level effects of bumetanide that, for instance, could change network excitability in the developing cortex and thus have large effects on protein translation and turnover[37]. Indeed, recent studies using sensory deprivation have

demonstrated generally similar effects on the synaptic proteome in the barrel cortex after whisker trimming in adult mice[30].

Many of the proteins that we found to be dysregulated in cortex of juvenile mice were previously defined as FMRP targets by known association of FMRP and their mRNAs[2]; however, these proteins were a relatively small fraction of the 842 confirmed targets[2], suggesting that other misexpressed proteins are due to pleiotropic or compensatory mechanisms. Therefore, it is possible that the altered development of E_{GABA} is a compensatory plasticity that itself is detrimental to the development of synapses and neural circuits. This might explain why mutations in several unrelated genes, with diverse functions, that underlie neurodevelopmental disorders all demonstrate changes in chloride homeostasis as a convergent cellular phenotype[32, 34]. Alternatively, it is possible that there are as yet untested molecular mechanisms that account for the altered chloride imbalance and GABA signaling after FMRP loss. For instance, FMRP is known to regulate miRNA expression and there are multiple miRNAs that are dysregulated in *Fmr1* KO mice[43], including known regulators of NKCC1[44], providing a plausible mechanism for changes in regulation of the chloride co-transporters.

Many of the synaptic perturbations, either functional or morphological, that have been described in the sensory cortex of *Fmr1* KO mice are present only during the CP and seem to normalize as mice develop[12, 13, 45]. However circuit level defects and abnormal sensory-related behaviors persist in adult mutant mice[8–10]. It has been speculated that the correct timing of the development of synapses during the CP is required for the refinement of the circuit early in development[46]. However, this has not been formally tested. Therefore, we addressed whether correction in the developmental profile of synapses during the CP was sufficient to restore the circuit alteration in mature cortex of *Fmr1* KO mice. We found that administration of bumetanide to mice limited to the CP was sufficient to correct the enhanced whisker-evoked responses in the barrel cortex of young adult *Fmr1* KO mice, which could have therapeutic implications for the symptom of sensory hypersensitivity and tactile defensiveness. It is important to note that while our cellular analysis has focused on layer IV spiny stellate neurons the intrinsic optical signal is the integration of many different responses of cortical neurons and interneurons. Therefore, the normalization of the map size and intensity suggests that the overall cortical response is corrected by bumetanide administered during the CP. This provides strong evidence that correcting synaptic maturation during the CP can have long lasting effects on the function of the circuit and supports the idea that the correct temporal refinement of synapses during early vulnerable periods is important to the correct function of the adult circuit. Prior work that has targeted metalloproteinases with minocycline to rescue dendritic spine development have also found that treatment during early development produces a long lasting improvement in some behaviors in *Fmr1* KO mice, further demonstrating the importance of intervention during the early CPs[47].

A previous study which also found a disruption of E_{GABA} in the hippocampus of *Fmr1* KO mice demonstrated that maternal pretreatment with bumetanide had effects on the behavior of neonates[48]. The authors found that prenatal treatment restored a transient hyperpolarization of E_{GABA} during parturition, which was dependent upon oxytocin

signaling. Furthermore, the abnormal chloride homeostasis in the hippocampus seemed to be dependent on the downregulation of KCC2[48]. Our findings support an alternative model that elevated NKCC1 is directly responsible for altered E_{GABA} in the cortex of *Fmr1* KO mice during the postnatal CP and this causes early synaptic deficits ultimately leading to long lasting circuit dysfunction. Bumetanide treatment during early vulnerable periods has also been shown to be effective in rescuing phenotypes in adult mice in a model of neonatal epileptic encephalopathy[49], further demonstrating that NKCC1 inhibition during postnatal CPs may be important in the treatment of diverse neurodevelopmental disorders.

In the current study, we have shown that systemic administration of bumetanide during the CP corrects synaptic maturation and plasticity and affects the synaptic proteome in *Fmr1* KO mice. Moreover, the early administration of this drug has a long lasting corrective effect on the function of the circuit in the sensory cortex. These studies provide further rationale for considering NKCC1 inhibitors for the use in neurodevelopmental disorders.

Experimental Procedures

Electrophysiology

Paracoronal sections containing the somatosensory cortex (400 μm) were prepared from male postnatal day (PND) 5–11 *Fmr1*$^{-/y}$ (*Fmr1* KO mice) and their male wild-type (WT) *Fmr1*$^{+/y}$ littermates (*Fmr1* WT mice). Mice were on a congenic C57BL/6 inbred background strain. Experiments and analysis were both performed with the experimenter blind to the genotype and treatment of the animal. Post hoc genotyping using DNA from tail biopsies was performed to confirm the genotype. Mice were anesthetized with isoflurane, decapitated, and the brain rapidly removed under ice-cold, oxygenated, sucrose-slicing ACSF containing 85 mM NaCl, 2.5 mM KCl, 1.2 mM NaH_2PO_4, 25 mM NaHCO3, 25mM glucose, 75 mM sucrose, 0.5 mM $CaCl_2$, and 4 mM $MgCl_2$, equilibrated with 95% O2/5% CO_2, and supplemented with the glutamate antagonists 100 μM kynurenate and 10 μM APV. Slices were incubated at 28 °C for 30 min, while slowly exchanging the sucrose ACSF in the incubation chamber for oxygenated sodium ACSF solution containing 125 mM NaCl, 2.4 mM KCl, 1.2 mM NaH_2PO_4, 25 mM $NaHCO_3$, 25 mM glucose, 1 mM CaCl2, and 2 mM MgCl2. After a recovery period of at least 1 hour, slices were transferred to a recording chamber positioned under an upright microscope where they were continuously perfused with oxygenated sodium ACSF containing 2mM $CaCl_2$ and 1 mM $MgCl_2$ and visualized with a 60x objective under DIC. Recordings were made from layer IV neurons in the somatosensory cortex at near physiological temperature (32°C). Spiny stellate cells are the most abundant neurons in layer IV [50] and were identified by their dense distribution in the walls of the barrel, their regular soma size (~10 μm), and morphology lacking a prominent apical dendrite[51].

For perforated patch clamp recording, borosilicate glass recording electrodes with resistances of 5–7 MΩ were filled with KCl solution containing 150 mM KCl, 10 mM HEPES, pH adjusted to 7.2 with Tris-OH. The pipette tip was filled with gramicidin-free KCl solution and then backfilled with solution containing gramicidin (100 μg/ml)[18]. The access resistance of the perforated cells was monitored, and 20MΩ was considered acceptable to start recording. Access resistance was monitored constantly during recordings,

and cells with a fluctuation of 15% were discarded. GABAergic currents were evoked in the presence of 50μM D-APV and 10μM CNQX using a glass monopolar extracellular stimulating electrode filled with ACSF positioned at the border of layer IV and V and recorded at holding potential between −80mV and +60 mV. The reversal potential of GABAergic currents was calculated from the intersection of the current-voltage curve with the *x*-axis.

For whole-cell patch clamp recordings electrodes were filled with the following internal solution 95 mM CsF, 25 mM CsCl, 10 mM Cs-HEPES, 10 mM Cs-EGTA, 2 mM NaCl, 2 mM Mg-ATP, 10 mM QX-314, 5 mM TEA-Cl, 5 mM 4-AP, pH adjusted to 7.3 with CsOH. A tungsten bipolar stimulating electrode was positioned in the ventrobasal thalamus and EPSCs isolated in spiny stellate neurons. Only stable evoked EPSC recordings that exhibited a constant latency were accepted as monosynaptic thalamocortical inputs[52]. Series resistance was continuously monitored using hyperpolarizing voltage steps generated by pClamp 9 software (Axon Instruments), and recordings were discarded if there was a >15% change during the course of the experiment. All recordings were made in the presence of $GABA_A$ receptor antagonists, picrotoxin (50μM), and bicuculline (10 μM). AMPA receptor mediated currents were measured as the peak current at a membrane potential of −70 mV and NMDA receptor mediated currents were recorded at +40mV, and measured in a 2.5ms window 60ms after the onset of the current.

To determine the fraction of silent synapses EPSCs were elicited by first determining a minimal stimulation intensity where an established synaptic connection exhibited a response failure rate of approximately 50% at −70 mV. This minimal stimulation was then used to elicit a response at −70 mV followed by a response at +40 mV in a single sweep.

For LTP experiments, the gramicidin perforated patch recording configuration was adopted to prevent LTP washout. Gramicidin (100 μg/ml) was added to our standard internal solution. Electrodes were tip filled with gramicidin-free internal and then backfilled with gamicidin-containing internal. After formation of a giga-ohm seal between the electrode and cell membrane, access resistance was continuously monitored using a hyperpolarizing step. Once stable access was reached (usually ~20 min) synaptic recordings were commenced. LTP was induced by pairing 100 stimuli at 1Hz with postsynaptic depolarization to 0 mV.

Data Analysis

Properties of EPSCs were analyzed using pClamp 10 (Axon). Genotypic and drug treatment comparisons were made using a two-way analysis of variance (ANOVA) followed by 2-tailed pairwise comparisons with Bonferroni adjustment for multiple comparisons unless otherwise stated. Normality of distribution was confirmed using Shapiro-Wilk test to satisfy the requirement for two-way ANOVA. For distributions that did not pass the normality test, we used nonparametric Kruskal Wallis H test followed by Mann Whitney U tests for pairwise comparisons. For LTP experiments, percentage potentiation was determined by averaging the EPSC amplitude during the last 5 min recording (25–30 min after LTP induction). Significance was determined by comparison of the last 5 min of baseline recording (prior to LTP induction) and the last 5 min of recording using a two-tailed unpaired *t*-test with the assumption of non equal variances. Two-tailed *t*-tests were

performed in other comparisons between two groups where indicated. Data are presented as mean ± SEM. Differences were considered significant when $p < 0.05$.

Drug Administration

Animals were housed in trio breeding with a male *Fmr1*$^{-/y}$ and two *Fmr1*$^{-/+}$ females. Births of new litters were monitored daily to ensure treatment started on the day of birth (PND 0). Intraperitoneal (i.p.) injections were made of bumetanide (0.20mg/kg), furosemide (20mg/kg), mannitol (750mg/kg). The vehicle used in for bumetanide was 0.9% saline and 0.1% ethanol, and for furosemide and mannitol experiments the vehicle was 0.9% saline. Minimal handling of pups and use of nestlets in cages was used to avoid disruption to new litters. For electrophysiology experiments, pups were injected daily from P0 until the day of experimentation. For OIS and mass spectrometry experiments, pups were injected from P0 to P14.

Cranial Windows

Chronic glass-covered cranial windows were implanted as previously described [53, 54]. Briefly, PND 14 mice were anesthetized with isoflurane (5% induction, 2% maintenance via nose cone) and placed in a stereotaxic frame over a warm water re-circulating blanket. Dexamethasone (0.2 mg/kg; Baxter Healthcare Corp.) and carprofen (5 mg/kg; Pfizer) were administered subcutaneously to reduce brain edema and local tissue inflammation. A 2–3 mm craniotomy was performed with a pneumatic dental drill. The center of the craniotomy was placed over the left hemisphere barrel cortex. A sterile round 5 mm glass cover slip (#1; Electron Microscopy Sciences) was gently laid over the dura matter and glued to the skull with cyanoacrylate-based glue. Dental acrylic was then applied to the skull surface and up to the wound edges. A titanium bar (0.125 × 0.375 × 0.05 inch) was embedded in the dental acrylic to secure the mouse on to the stage for imaging. Following recovery for ~1 h, mouse pups were returned to their cages with their dam and littermates.

Optical intrinsic signal imaging

Optical intrinsic signal (OIS) imaging of the D2 whisker (D2W) sensory receptive field was done at two different time points in the same mice: PND 16–17 and at 2 months (not all mice were imaged at both times due to window clarity issues). Whiskers surrounding the D2W were gently trimmed with Vannas scissors (down to a length of ~ 2 mm) just prior to imaging to facilitate single whisker stimulation. OIS imaging was performed through the cranial window on mice under light anesthesia with 0.5–0.75% isoflurane and a single dose of chlorprothixene (3 mg/kg, i.p., Sigma-Aldrich). The cortical surface was illuminated by green (535 nm) and red (630 nm) light-emitting diodes (LEDs) mounted around a ‘front-to-front’ tandem arrangement of objective lenses (135 mm and 50 mm focal lengths, Nikon). The green LEDs were used to visualize the superficial vasculature and the red LEDs were used for IOS imaging. The microscope was focused to ~350 μm below the cortical surface for 2 month mice and about ~300 μm for P16–17 mice. Imaging was performed at 10 Hz using a fast camera (Pantera 1M60, Dalsa), frame grabber (64 Xcelera-CL PX4, Dalsa) and custom routines written in MATLAB. Each session consisted of 30 trials (at 10 s intervals) of mechanical stimulation for 1.5 s (100 Hz) using a glass micropipette coupled to a piezo bender actuator (Physik Instrumente). Frames 0.9 s before the onset of stimulation (baseline)

and 1.5 s after stimulation (response) were collected. Frames were binned 3 times temporally and 2 × 2 spatially. Stimulated cortical areas were identified by dividing the response signal by the averaged baseline signal (DR/R) for every trial and then summing all trials. Response maps were then thresholded at 50% of maximum response to get the responsive cortical areas for D2W. For a subset of mice and time points, maps at different depths were averaged to account for slight variations in signal.

Analysis for OIS

Cortical sensory representation map sizes were defined by ImageJ software (National Institutes of Health, Bethesda, MD). To compute statistical differences between genotype and treatment interactions, two-way ANOVAs were performed followed by 2-tailed pairwise comparisons with Bonferroni corrections. For comparisons between WT bumetanide - *Fmr1* KO vehicle and WT vehicle – *Fmr1* KO bumetanide groups, T-Tests for independent samples with Bonferroni correction (alpha = 0.05 / 2; confidence level = 97.5%) were used to compute statistical differences. All statistical tests were conducted in SPSS 23 software (IBM Corporation, USA). All data are presented as the mean ± standard error of the mean. Significance was set at $p < 0.05$*, $p < 0.001$**, $p < 0.0001$***.

Quantitative Proteomics and Analysis

Barrel cortices from *Fmr1* KO and WT mice treated with either bumetanide or vehicle were homogenized and lysed in 6 M guanidine, 100 mM HEPES, pH = 8.5. Samples were heated to 95 °C for three minutes. Next the proteins were reduced at 5 mM DTT for 20 mins and alkylated at 15 mM iodoacetamide for 20 mins. The reaction was quenched by adding DTT to 50 mM and incubation for 15 mins. The solution was then diluted to 50 mM HEPES, 1.5 M Guanidine. 1 μg of Lys-C protease (Pierce) was added to each sample and incubated for three hours at room temperature whilst vortexing. 2 μg of trypsin protease (Pierce) was added next and samples were incubated overnight at 37 °C whilst vortexing. Following digestion, the samples were acidified 0.5% TFA, bound to alkylated resin (Pierce C18 spin columns), and washed with 5% acetonitrile, 0.5% TFA. Samples were eluted from resin with 80% acetonitrile, 0.5% formic acid buffer. Eluted samples were dried down using vacuum centrifugation, and resuspended in 50mM HEPES. MicroBCA (Pierce) was used to determine peptide mass concentration. 80 μg of each sample were aliquoted for TMT labeling with 0.4mg of a respective TMT label (Thermo Scientific). For each of vehicle and bumetanide treatment, the samples were labeled as follows: 5xFmr1 WT to labels 126, 127n, 127c, 128n, and 128c respectively; and 5x *Fmr1* KO to labels 129n, 129c, 130n, 130c, 131 respectively. Labeling reaction took place for one hour and 15 mins at room temperature. Reaction was quenched by bringing sample solutions to 0.3% (v/v) hydroxylamine and incubated for fifteen minutes at room temperature. The ten samples (for each treatment) were then combined at a ratio of 1:1:1:1:1:1:1:1:1:1. The combined samples were then acidified to 0.5% TFA, bound to alkylated resin (HyperSep C18 vacuum cartridges), and washed with 5% acetonitrile, 0.5% TFA before being eluted with 80% acetonitrile, 0.5% formic acid. Eluted combinatory samples were dried down using vacuum centrifugation, and subsequently resuspended in 0.1% TFA. Samples were fractionated using strong cation exchange nitrocellulose spin columns (Pierce). Six elution fractions for each sample were created corresponding to 50 mM sodium acetate (NaAcO), 100 mM NaAcO, 250 mM

NaAcO, 500 mM NaAcO, 1 M NaAcO, and 4 M NaAcO. Every fraction was desalted by acidification to pH = 2 with TFA, binding to alkylated resin (Pierce C18 spin columns), washing with 5% acetonitrile, 0.5% TFA and eluted with 80% acetonitrile, 0.5% formic acid. Fractions were dried using vacuum centrifugation, and resuspended in LCMS Buffer A: 5% acetonitrile, 0.125% formic acid. Fractions were quantified using microBCA (Pierce).

3 μg from each fraction were loaded for LC-MS analysis using a Thermo Orbitrap Fusion coupled to a Thermo EASY nLC-1200 UPLC pump and vented Acclaim Pepmap 100, 75 μm × 2 cm nanoViper trap column and nanoViper analytical column: Thermo – 164570, 3 μm, 100 Å, C18, 0.075 mm, 500 mm with stainless steel emitter tip assembled on the Nanospray Flex Ion Source with a spray voltage of 2000V. For the chromatographic run, Buffer A contained [as above] and Buffer B contained 95% acetonitrile, 0.125% formic acid. A four-hour gradient was established beginning with 100% A, 0% B and increased to 7% B over 5 mins, then to 25% B over 160 mins, 36% B over 40 mins, 45% B over 10 mins, 95% B over 10 mins, and held at 95% B for 15 mins before terminating the scan. The multinotch MS3 method[55] parameters include: Ion transfer tube temp = 300°C, Easy-IC internal mass calibration, default charge state = 2 and cycle time =3 s. MS1 detector set to orbitrap with 60K resolution, wide quad isolation, mass range = normal, scan range = 300–1800 m/z, max injection time = 50ms, AGC target = $2*10^5$, microscans =1, RF lens = 60%, without source fragmentation, and datatype = positive and centroid. MIPS was set as on, included charge states 2–7 and reject unassigned. Dynamic exclusion was enabled with n=1 exclusion for 60s with 10ppm tolerance for high and low. An intensity threshold was set to $5*10^3$. Precursor selection decision = most intense, top speed, 3s. MS2 settings include isolation window = 0.7, scan range = auto normal, collision energy = 35% CID, scan rate = turbo, max injection time = 50ms, AGC target = $1*10^4$, Q = 0.25. The top ten precursors were selected for MS3 analysis. Precursors were fragmented using 65% HCD before orbitrap detection. A precursor selection range of 400–1200 m/z was chosen with mass range tolerance. An exclusion mass width was set to 18 ppm on the low and 5 ppm on the high. Isobaric tag loss exclusion was set to TMT reagent. Additional MS3 settings include an isolation window = 2, orbitrap resolution = 60K, scan range = 120 – 500 m/z, AGC target = $1*10^4$, max injection time = 120 ms, microscans =1, and data type = profile.

Spectral raw files were extracted into MS1, MS2, and MS3 files using the in-house program RawConverter[56]. Spectral files were pooled from fractions and an unfractionated portion for each sample and searched against the Uniprot mouse protein database (reviewed_iso_cont_3_25_14) and matched to sequences using the ProLuCID/SEQUEST algorithm (ProLuCID ver. 3.1) with 50 ppm peptide mass tolerance for precursor ions and 600ppm for fragment ions. The search space included all fully and half-tryptic peptide candidates that fell within the mass tolerance window with no miscleavage constraint, assembled and filtered with DTASelect2 (ver. 2.1.3) through the Integrated Proteomics Pipeline (IP2 v.5.0.1, Integrated Proteomics Applications, Inc., CA, USA). Static modifications included 57.02146 C and 229.162932 K and N-term. Peptide probabilities and false-discovery ratios were produced using a target/decoy approach. Each protein identified was required to have a minimum of one peptide of minimal length five. A false discovery rate of 1% was used for data filtering. Isobaric labeling analysis was performed with Census

2 as previously described[57]. TMT channels were normalized by dividing it over the sum of all channels. No intensity threshold was applied.

To calculate the fold change KO vs. WT, the normalized average intensity values for proteins from Census were used and the values were standardized to the mean of the five WT samples. The fold change could then be calculated as the mean of the KO standardized values. *P* values were calculated by Student's *t*-test. For Panther analysis, the list of significantly upregulated proteins was queried against all proteins quantified in the dataset using a statistical overrepresentation test of the GO biological process complete annotation[31]. Biological processes which were a subset of a larger group that was also statistically significant were defaulted to the more encompassing annotation and its associated *p* value.

Supplementary Material

Refer to Web version on PubMed Central for supplementary material.

Acknowledgments

We thank Dr. Máté Marosi for help with the intrinsic signal imaging experiments. This work was funded by grants from NIH/NIMH (1R21MH104808) to AC, DOD USAMRMC W81XWH-14-1-0433 and a John Merck Fund award to AC and CP-C, the Simons Foundation (SFARI Award 295438) and NIH/NICHD (5R01HD054453) to CP-C. JNS was supported by NIH/NIDCD (R00DC-013805) and The Hartwell Foundation. QH was supported by a fellowship from the FRAXA Research Foundation. Data from LC-MS experiments were uploaded to a public repository ftp://MSV000081526@massive.ucsd.edu

References

1. Penagarikano O, Mulle JG, Warren ST. The pathophysiology of fragile x syndrome. Annu Rev Genomics Hum Genet. 2007; 8:109–129. [PubMed: 17477822]
2. Darnell JC, Van Driesche SJ, Zhang C, Hung KY, Mele A, Fraser CE, et al. FMRP stalls ribosomal translocation on mRNAs linked to synaptic function and autism. Cell. 2011; 146(2):247–261. [PubMed: 21784246]
3. Contractor A, Klyachko VA, Portera-Cailliau C. Altered Neuronal and Circuit Excitability in Fragile X Syndrome. Neuron. 2015; 87(4):699–715. [PubMed: 26291156]
4. Kau AS, Meyer WA, Kaufmann WE. Early development in males with Fragile X syndrome: a review of the literature. Microsc Res Tech. 2002; 57(3):174–178. [PubMed: 12112454]
5. Baranek GT, Foster LG, Berkson G. Tactile defensiveness and stereotyped behaviors. Am J Occup Ther. 1997; 51(2):91–95. [PubMed: 9124275]
6. Cascio CJ. Somatosensory processing in neurodevelopmental disorders. J Neurodev Disord. 2010; 2(2):62–69. [PubMed: 22127855]
7. Rotschafer S, Razak K. Altered auditory processing in a mouse model of fragile X syndrome. Brain Res. 2013; 1506:12–24. [PubMed: 23458504]
8. Arnett MT, Herman DH, McGee AW. Deficits in tactile learning in a mouse model of fragile X syndrome. PLoS One. 2014; 9(10):e109116. [PubMed: 25296296]
9. Zhang Y, Bonnan A, Bony G, Ferezou I, Pietropaolo S, Ginger M, et al. Dendritic channelopathies contribute to neocortical and sensory hyperexcitability in Fmr1(−/y) mice. Nat Neurosci. 2014; 17(12):1701–1709. [PubMed: 25383903]
10. He CX, Cantu DA, Mantri SS, Zeiger WA, Goel A, Portera-Cailliau C. Tactile Defensiveness and Impaired Adaptation of Neuronal Activity in the Fmr1 Knock-Out Mouse Model of Autism. J Neurosci. 2017; 37(27):6475–6487. [PubMed: 28607173]

11. Goncalves JT, Anstey JE, Golshani P, Portera-Cailliau C. Circuit level defects in the developing neocortex of Fragile X mice. Nat Neurosci. 2013; 16(7):903–909. [PubMed: 23727819]
12. Harlow EG, Till SM, Russell TA, Wijetunge LS, Kind P, Contractor A. Critical period plasticity is disrupted in the barrel cortex of FMR1 knockout mice. Neuron. 2010; 65(3):385–398. [PubMed: 20159451]
13. Cruz-Martin A, Crespo M, Portera-Cailliau C. Delayed stabilization of dendritic spines in fragile X mice. J Neurosci. 2010; 30(23):7793–7803. [PubMed: 20534828]
14. Bureau I, Shepherd GM, Svoboda K. Circuit and plasticity defects in the developing somatosensory cortex of FMR1 knock-out mice. J Neurosci. 2008; 28(20):5178–5188. [PubMed: 18480274]
15. Patel AB, Hays SA, Bureau I, Huber KM, Gibson JR. A target cell-specific role for presynaptic Fmr1 in regulating glutamate release onto neocortical fast-spiking inhibitory neurons. J Neurosci. 2013; 33(6):2593–2604. [PubMed: 23392687]
16. Crair MC, Malenka RC. A critical period for long-term potentiation at thalamocortical synapses. Nature. 1995; 375(6529):325–328. [PubMed: 7753197]
17. Inan M, Crair MC. Development of cortical maps: perspectives from the barrel cortex. Neuroscientist. 2007; 13(1):49–61. [PubMed: 17229975]
18. He Q, Nomura T, Xu J, Contractor A. The developmental switch in GABA polarity is delayed in fragile X mice. J Neurosci. 2014; 34(2):446–450. [PubMed: 24403144]
19. Wang DD, Kriegstein AR. Defining the role of GABA in cortical development. J Physiol. 2009; 587(Pt 9):1873–1879. [PubMed: 19153158]
20. Ben-Ari Y, Gaiarsa JL, Tyzio R, Khazipov R. GABA: a pioneer transmitter that excites immature neurons and generates primitive oscillations. Physiol Rev. 2007; 87(4):1215–1284. [PubMed: 17928584]
21. Kaila K, Price TJ, Payne JA, Puskarjov M, Voipio J. Cation-chloride cotransporters in neuronal development, plasticity and disease. Nat Rev Neurosci. 2014; 15(10):637–654. [PubMed: 25234263]
22. Chancey JH, Adlaf EW, Sapp MC, Pugh PC, Wadiche JI, Overstreet-Wadiche LS. GABA depolarization is required for experience-dependent synapse unsilencing in adult-born neurons. J Neurosci. 2013; 33(15):6614–6622. [PubMed: 23575858]
23. Oh WC, Lutzu S, Castillo PE, Kwon HB. De novo synaptogenesis induced by GABA in the developing mouse cortex. Science (New York, NY). 2016; 353(6303):1037–1040.
24. Deidda G, Allegra M, Cerri C, Naskar S, Bony G, Zunino G, et al. Early depolarizing GABA controls critical-period plasticity in the rat visual cortex. Nat Neurosci. 2015; 18(1):87–96. [PubMed: 25485756]
25. Cleary RT, Sun H, Huynh T, Manning SM, Li Y, Rotenberg A, et al. Bumetanide enhances phenobarbital efficacy in a rat model of hypoxic neonatal seizures. PLoS One. 2013; 8(3):e57148. [PubMed: 23536761]
26. Loscher W, Puskarjov M, Kaila K. Cation-chloride cotransporters NKCC1 and KCC2 as potential targets for novel antiepileptic and antiepileptogenic treatments. Neuropharmacology. 2013; 69:62–74. [PubMed: 22705273]
27. Isaac JT, Crair MC, Nicoll RA, Malenka RC. Silent synapses during development of thalamocortical inputs. Neuron. 1997; 18(2):269–280. [PubMed: 9052797]
28. Tang B, Wang T, Wan H, Han L, Qin X, Zhang Y, et al. Fmr1 deficiency promotes age-dependent alterations in the cortical synaptic proteome. Proc Natl Acad Sci U S A. 2015; 112(34):E4697–4706. [PubMed: 26307763]
29. Li Z, Adams RM, Chourey K, Hurst GB, Hettich RL, Pan C. Systematic comparison of label-free, metabolic labeling, and isobaric chemical labeling for quantitative proteomics on LTQ Orbitrap Velos. J Proteome Res. 2012; 11(3):1582–1590. [PubMed: 22188275]
30. Butko MT, Savas JN, Friedman B, Delahunty C, Ebner F, Yates JR 3rd, et al. In vivo quantitative proteomics of somatosensory cortical synapses shows which protein levels are modulated by sensory deprivation. Proc Natl Acad Sci U S A. 2013; 110(8):E726–735. [PubMed: 23382246]

31. Mi H, Poudel S, Muruganujan A, Casagrande JT, Thomas PD. PANTHER version 10: expanded protein families and functions, and analysis tools. Nucleic Acids Res. 2016; 44(D1):D336–342. [PubMed: 26578592]
32. Deidda G, Parrini M, Naskar S, Bozarth IF, Contestabile A, Cancedda L. Reversing excitatory GABAAR signaling restores synaptic plasticity and memory in a mouse model of Down syndrome. Nat Med. 2015; 21(4):318–326. [PubMed: 25774849]
33. Tang X, Kim J, Zhou L, Wengert E, Zhang L, Wu Z, et al. KCC2 rescues functional deficits in human neurons derived from patients with Rett syndrome. Proc Natl Acad Sci U S A. 2016; 113(3):751–756. [PubMed: 26733678]
34. Banerjee A, Rikhye RV, Breton-Provencher V, Tang X, Li C, Li K, et al. Jointly reduced inhibition and excitation underlies circuit-wide changes in cortical processing in Rett syndrome. Proc Natl Acad Sci U S A. 2016; 113(46):E7287–E7296. [PubMed: 27803317]
35. Li Y, Cleary R, Kellogg M, Soul JS, Berry GT, Jensen FE. Sensitive isotope dilution liquid chromatography/tandem mass spectrometry method for quantitative analysis of bumetanide in serum and brain tissue. J Chromatogr B Analyt Technol Biomed Life Sci. 2011; 879(13–14):998–1002.
36. Topfer M, Tollner K, Brandt C, Twele F, Broer S, Loscher W. Consequences of inhibition of bumetanide metabolism in rodents on brain penetration and effects of bumetanide in chronic models of epilepsy. Eur J Neurosci. 2014; 39(4):673–687. [PubMed: 24251546]
37. Owens DF, Kriegstein AR. Is there more to GABA than synaptic inhibition? Nat Rev Neurosci. 2002; 3(9):715–727. [PubMed: 12209120]
38. Lombardi LM, Baker SA, Zoghbi HY. MECP2 disorders: from the clinic to mice and back. J Clin Invest. 2015; 125(8):2914–2923. [PubMed: 26237041]
39. Benowitz LI, Routtenberg A. GAP-43: an intrinsic determinant of neuronal development and plasticity. Trends Neurosci. 1997; 20(2):84–91. [PubMed: 9023877]
40. Itami C, Kimura F, Nakamura S. Brain-derived neurotrophic factor regulates the maturation of layer 4 fast-spiking cells after the second postnatal week in the developing barrel cortex. J Neurosci. 2007; 27(9):2241–2252. [PubMed: 17329421]
41. Wen TH, Afroz S, Reinhard SM, Palacios AR, Tapia K, Binder DK, et al. Genetic Reduction of Matrix Metalloproteinase-9 Promotes Formation of Perineuronal Nets Around Parvalbumin-Expressing Interneurons and Normalizes Auditory Cortex Responses in Developing Fmr1 Knock-Out Mice. Cereb Cortex. 2017:1–14. [PubMed: 28365777]
42. Nomura T, Musial TF, Marshall JJ, Zhu Y, Remmers CL, Xu J, et al. Delayed Maturation of Fast-Spiking Interneurons Is Rectified by Activation of the TrkB Receptor in the Mouse Model of Fragile X Syndrome. J Neurosci. 2017; 37(47):11298–11310. [PubMed: 29038238]
43. Liu T, Wan RP, Tang LJ, Liu SJ, Li HJ, Zhao QH, et al. A MicroRNA Profile in Fmr1 Knockout Mice Reveals MicroRNA Expression Alterations with Possible Roles in Fragile X Syndrome. Mol Neurobiol. 2015; 51(3):1053–1063. [PubMed: 24906954]
44. Lippi G, Fernandes CC, Ewell LA, John D, Romoli B, Curia G, et al. MicroRNA-101 Regulates Multiple Developmental Programs to Constrain Excitation in Adult Neural Networks. Neuron. 2016
45. Nimchinsky EA, Oberlander AM, Svoboda K. Abnormal development of dendritic spines in FMR1 knock-out mice. J Neurosci. 2001; 21(14):5139–5146. [PubMed: 11438589]
46. Meredith RM. Sensitive and critical periods during neurotypical and aberrant neurodevelopment: a framework for neurodevelopmental disorders. Neurosci Biobehav Rev. 2015; 50:180–188. [PubMed: 25496903]
47. Dansie LE, Phommahaxay K, Okusanya AG, Uwadia J, Huang M, Rotschafer SE, et al. Long-lasting effects of minocycline on behavior in young but not adult Fragile X mice. Neuroscience. 2013; 246:186–198. [PubMed: 23660195]
48. Tyzio R, Nardou R, Ferrari DC, Tsintsadze T, Shahrokhi A, Eftekhari S, et al. Oxytocin-mediated GABA inhibition during delivery attenuates autism pathogenesis in rodent offspring. Science. 2014; 343(6171):675–679. [PubMed: 24503856]

49. Marguet SL, Le-Schulte VTQ, Merseburg A, Neu A, Eichler R, Jakovcevski I, et al. Treatment during a vulnerable developmental period rescues a genetic epilepsy. Nat Med. 2015; 21(12): 1436–1444. [PubMed: 26594844]
50. Feldmeyer D, Egger V, Lubke J, Sakmann B. Reliable synaptic connections between pairs of excitatory layer 4 neurones within a single 'barrel' of developing rat somatosensory cortex. J Physiol. 1999; 521 Pt 1:169–190. [PubMed: 10562343]
51. Daw MI, Ashby MC, Isaac JT. Coordinated developmental recruitment of latent fast spiking interneurons in layer IV barrel cortex. Nat Neurosci. 2007; 10(4):453–461. [PubMed: 17351636]
52. Feldman DE, Nicoll RA, Malenka RC, Isaac JT. Long-term depression at thalamocortical synapses in developing rat somatosensory cortex. Neuron. 1998; 21(2):347–357. [PubMed: 9728916]
53. Mostany R, Portera-Cailliau C. A method for 2-photon imaging of blood flow in the neocortex through a cranial window. J Vis Exp. 2008; (12)
54. Holtmaat A, de Paola V, Wilbrecht L, Trachtenberg JT, Svoboda K, Portera-Cailliau C. Imaging neocortical neurons through a chronic cranial window. Cold Spring Harb Protoc. 2012; 2012(6): 694–701. [PubMed: 22661440]
55. McAlister GC, Nusinow DP, Jedrychowski MP, Wuhr M, Huttlin EL, Erickson BK, et al. MultiNotch MS3 enables accurate, sensitive, and multiplexed detection of differential expression across cancer cell line proteomes. Anal Chem. 2014; 86(14):7150–7158. [PubMed: 24927332]
56. He L, Diedrich J, Chu YY, Yates JR 3rd. Extracting Accurate Precursor Information for Tandem Mass Spectra by RawConverter. Anal Chem. 2015; 87(22):11361–11367. [PubMed: 26499134]
57. Park SK, Aslanian A, McClatchy DB, Han X, Shah H, Singh M, et al. Census 2: isobaric labeling data analysis. Bioinformatics. 2014; 30(15):2208–2209. [PubMed: 24681903]

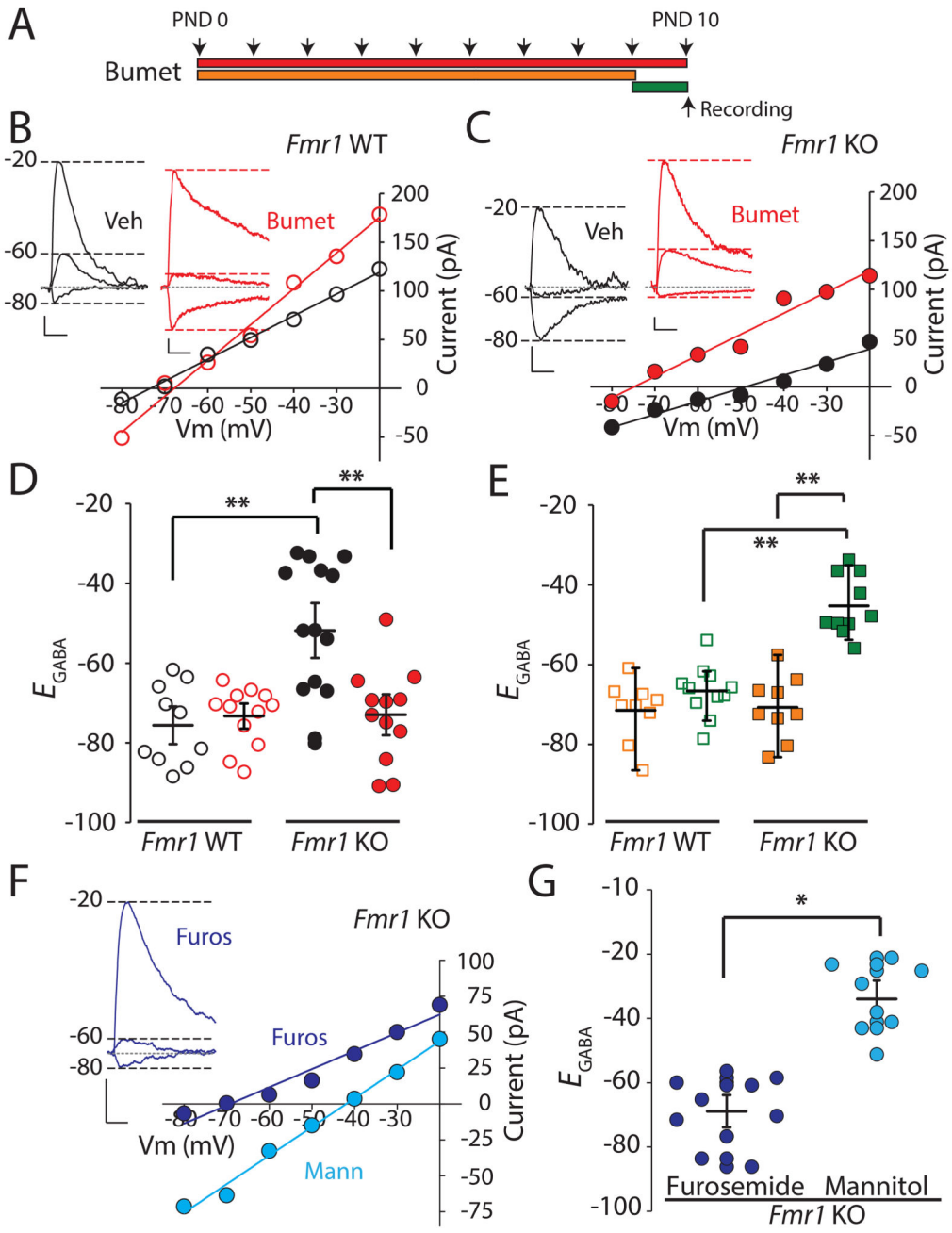

Figure 1. NKCC1 inhibition During the Critical Period Corrects E_{GABA} in the Somatosensory Cortex of *Fmr1* KO mice

(A) Schematic of different bumetanide treatment regimes: red bar, daily injections of 0.2mg/kg bumetanide from PND 0 to PND 10; orange bar, daily bumetanide treatment from P0 to P9; green bar, single dose of bumetanide on the day of the experiment (PND 10). (B) Representative current against voltage (I/V) plots of evoked GABA IPSCs in layer IV neurons from PND 10 *Fmr1* WT mice with 10 day bumetanide (red) or vehicle treatment (black). Insert: representative traces of GABA IPSCs recorded at Vm −80mV, −60mV and −20mV in vehicle and bumetanide treated neurons. Calibration: 20ms, 20pA (C) I/V plots of GABA IPSCs from layer IV neurons from *Fmr1* KO mice at PND 10. Representative GABA

current traces are shown. Calibration: 20ms, 20pA (D) Grouped data from all experiments of E_{GABA} estimated from the IV plots from *Fmr1* WT and *Fmr1* KO mice (E) E_{GABA} calculated from recordings of neurons in *Fmr1* WT and *Fmr1* KO mice after 9 day treatment (orange), and single dose administration (green) (F) I/V plots of IPSCs in layer IV neurons from furosemide (blue) and mannitol (cyan) (10 day) treated *Fmr1* KO mice recorded at PND 10 with inset representative trace from one furosemide treated mouse. Calibration: 20 ms, 20 pA. (G) E_{GABA} calculated from all recordings in *Fmr1* KO in furosemide group (blue) and mannitol group (cyan). * $p < 0.05$, ** $p < 0.01$ using two-way ANOVA with 2-tailed pairwise comparisons and Bonferroni adjustment for multiple comparisons. Comparison for (G) was conducted with unpaired T-test.

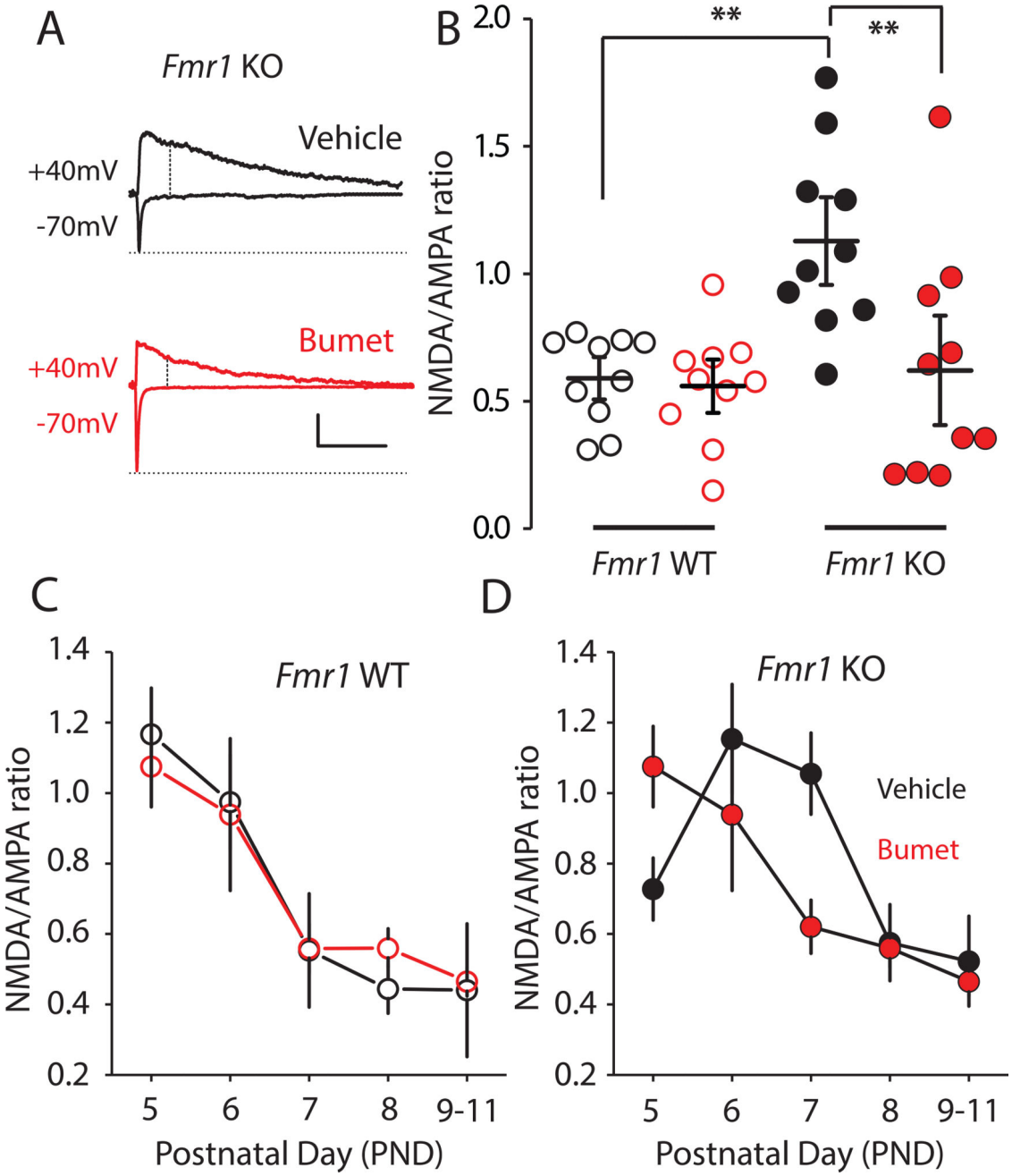

Figure 2. Bumetanide corrects developmental progression of synaptic transmission

(A) Representative EPSCs from *Fmr1* KO vehicle treated (black) or bumetanide treated (red) groups at PND 7. AMPAR mediated EPSCs were measured as the peak current at Vm −70 mV. The NMDAR component was recorded at Vm +40 mV and measured as the mean current over a 2.5ms window, 60 ms after the onset of the outward current. Calibration: 100 ms, 200 pA. (B) Grouped data of N:A ratio from the *Fmr1* WT vehicle group n = 10/4; *Fmr1* WT bumetanide group n=10/4; *Fmr1* KO vehicle group n = 10/7; *Fmr1* KO bumetanide group n = 10/8. (C) Time course of the development in N:A ratio at thalamocortical synapses in vehicle and bumetanide treated *Fmr1* WT mice from PND 5 to PND 11. (D)

Time course of development of the N:A ratio at thalamocortical synapses in vehicle and bumetanide-treated *Fmr1* KO mice from PND 5 to PND 11. All values are mean ± s.e.m. ** denotes $p < 0.01$ using two-way ANOVA with 2-tailed pairwise comparisons and Bonferroni adjustment for multiple comparisons.

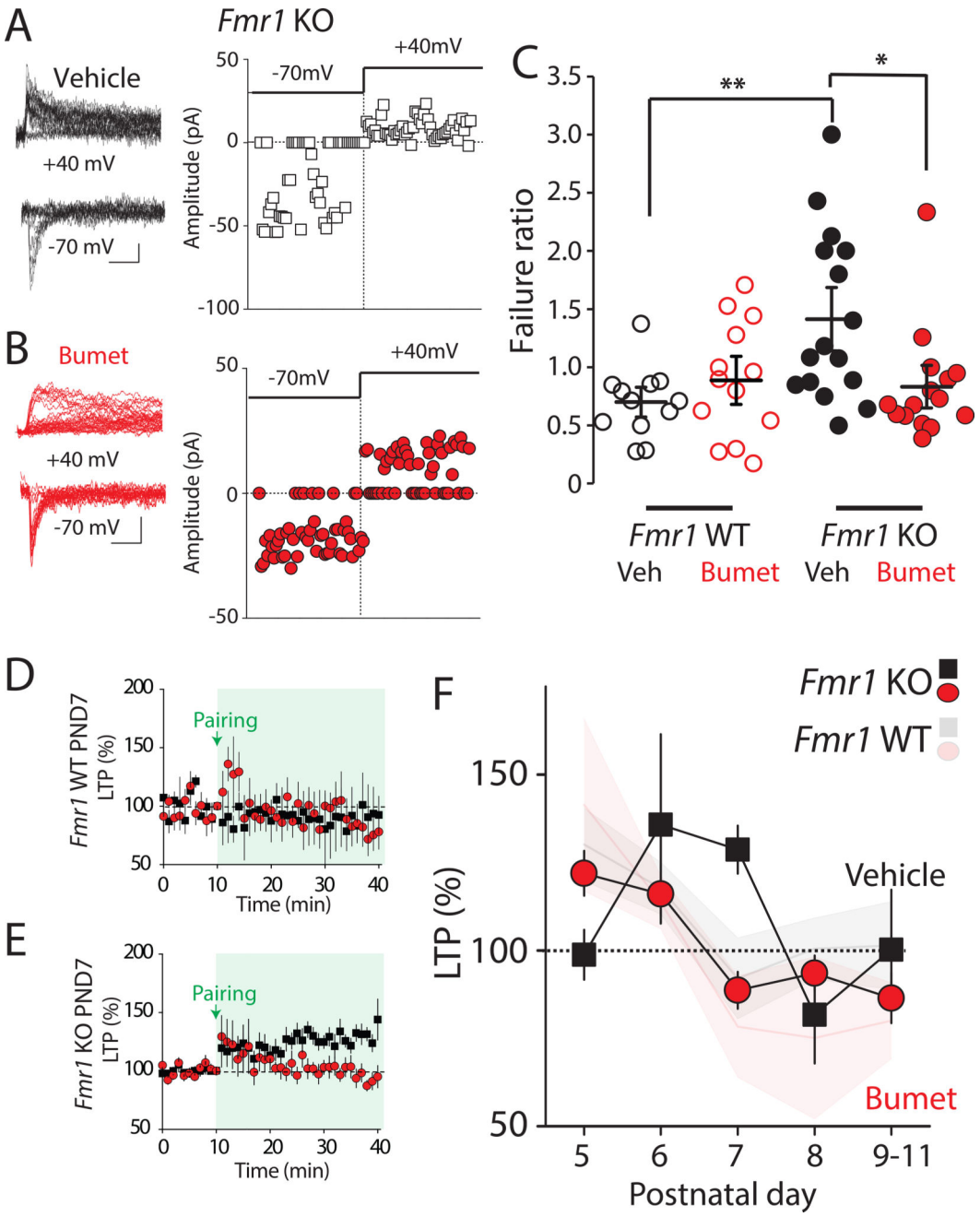

Figure 3. Persistent silent synapses and LTP expression beyond the critical period are corrected by NKCC1 inhibition

(A) Representative traces and EPSC amplitudes from a single experiment in vehicle treated *Fmr1* KO mice. Calibration: 20pA, 50ms. AMPA and NMDA failure rate were measured at −70 mV and +40mV respectively. (B) Representative traces and amplitudes from a single experiment in bumetanide treated *Fmr1* KO mice. (C) Grouped data from all experiments of the calculated failure ratio (Failures at −70 mV/ Failures at +40 mV). Box plots indicate top and bottom quartiles; whiskers specify top and bottom 10–90%. * $p < 0.05$, ** $p < 0.01$ Kruskal Wallis H test with Mann-Whitney U test for pairwise comparisons. (E) Grouped time course of thalamocortical LTP in vehicle or bumetanide treated *Fmr1* WT and *Fmr1*

KO mice at PND 7. All values are mean ± s.e.m. (F) Temporal progression of thalamocortical LTP from grouped data of vehicle and bumetanide treated *Fmr1* KO mice at each postnatal day between P5 and P11. Opaque graphs are LTP progression in *Fmr1* WT in vehicle and bumetanide. All values are mean ± s.e.m * $p < 0.05$ Two way ANOVA.

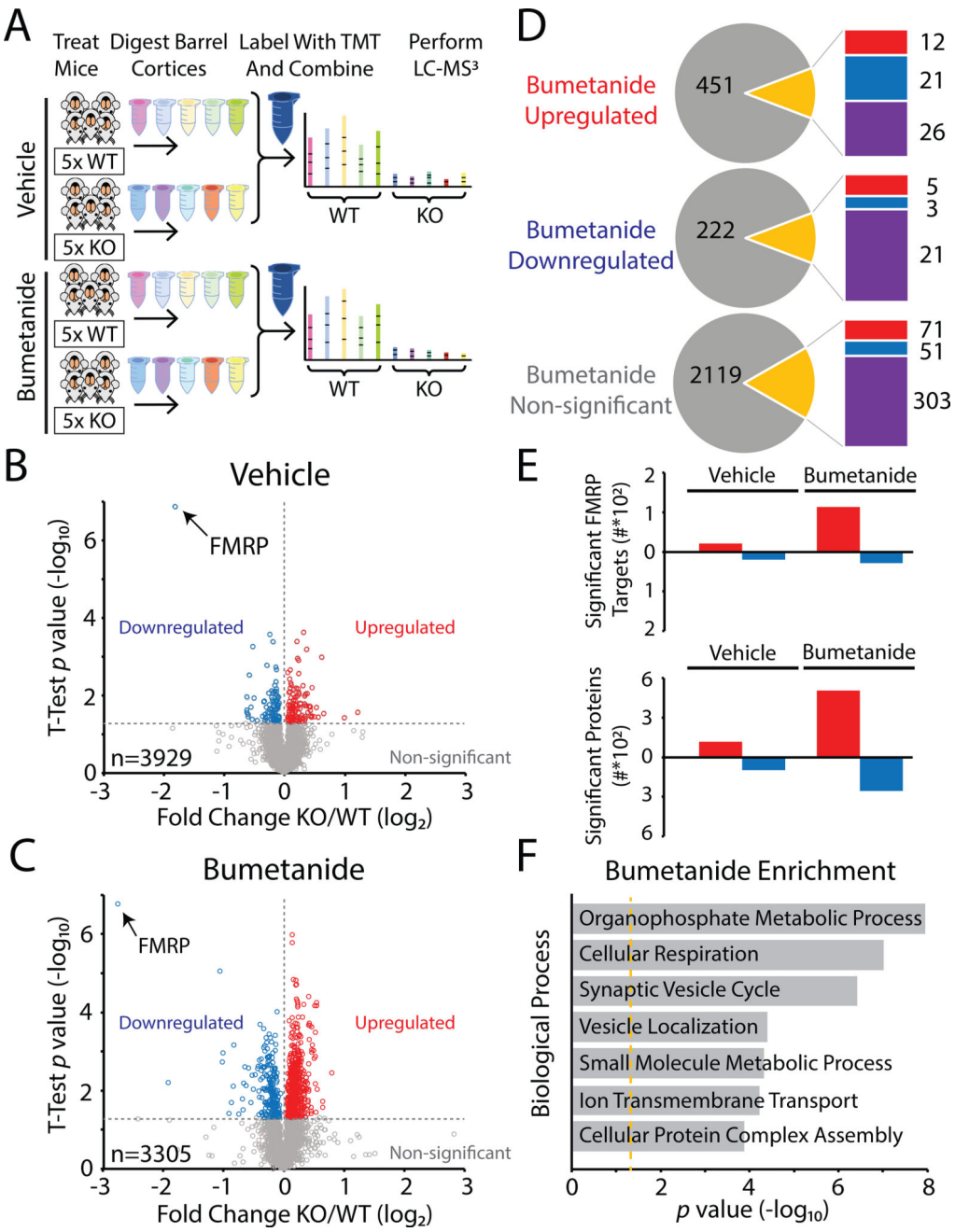

Figure 4. The proteome is remodeled by bumetanide treatment during the critical period

Proteomic analysis of sensory cortex in bumetanide treated *Fmr1* KO and WT mice. (A) Schematic of experimental workflow of proteomics protocol. Groups of *Fmr1* KO and *Fmr1* WT were administered vehicle or bumetanide from P0 to P14 covering the CP when the Cl^- equilibrium potential is relatively depolarized. The barrel cortices were isolated using tissue punches at P17 and proteins were subsequently digested into peptides. The ten samples each of vehicle or bumetanide groups were labeled with TMT and then combined and analyzed by MS^3 multinotch LC-MS to determine protein fold differences between *Fmr1* KO mice and *Fmr1* WT mice. (B) Volcano plot showing the protein level fold change relative to

significance between *Fmr1* KO and *Fmr1* WT mice in vehicle and (C) bumetanide treatment groups. Significantly upregulated proteins are in red (p value < 0.05), significantly downregulated proteins are in blue (p value < 0.05), and all other proteins are in gray. (D) Pie charts describing how the all proteins in the bumetanide group (significantly upregulated,top; significantly downregulated, middle; or non-significant) were found in the vehicle treated group comparison (p value < 0.05). Gray indicates proteins in vehicle that were not significantly different, while red and blue indicate significantly upregulated and downregulated in the vehicle groups respectively (purple are proteins found in the bumetanide samples but not identified in the vehicle groups). (E) Bar graphs showing the number of proteins either upregulated (red) or downregulated (blue) in either vehicle or bumetanide treatment groups. A subset of these proteins is presumed to be directly regulated by FMRP[2]. (F) Panther analysis of statistically overrepresented biological processes amongst bumetanide upregulated proteins. Orange line indicates Bonferroni corrected p value = 0.05. Shown as a rank ordered list of most significant general biological processes.

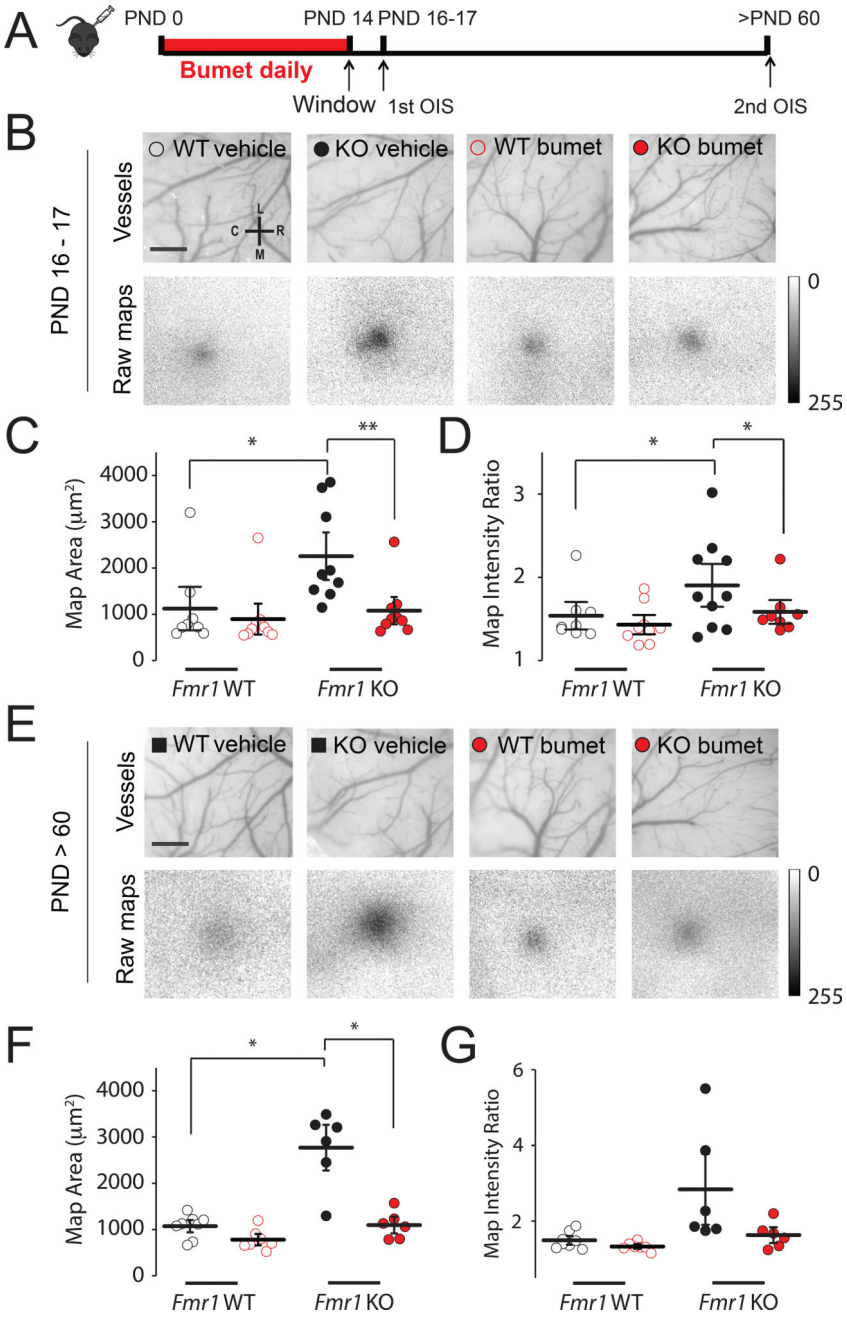

Figure 5. Long lasting correction of cortical whisker evoked responses after critical period treatment with bumetanide

(A) Schematic representation of time-course of OIS experiments. (B) Top: vasculature of S1 somatosensory cortex of PND 16–17 *Fmr1* WT and *Fmr1* KO mice; Bottom: corresponding cortical excitation maps collected during D2 whisker stimulation. Calibration: 0.5 mm (C) Map area measured in PND 16–17 *Fmr1* WT and *Fmr1* KO mice in vehicle (black) and bumetanide (red). (D) Map intensity ratio measured in PND 16–17 mice. (E) Vasculature and cortical excitation maps for mice PND > 60; same representative mice as shown in (B). Calibration: 0.5 mm (F) Map area measured in mice (G) Map intensity ratio measured in

mature mice. Significance was determined using two-way ANOVA with Bonferroni correction *$p < 0.05$ ** $p < 0.01$.